

Thickness determination of hydroperoxidized lipid bilayers from medium-resolution cryo-TEM images

Eulalie Lafarge^a, Carlos M. Marques^b, Marc Schmutz^a, Pierre Muller^a, and André P. Schroder^{c,*}

^aInstitut Charles Sadron, CNRS UPR22 — University of Strasbourg, 23 rue du Loess, Strasbourg, 67034, France

^bENS–Lyon, Chemistry Laboratory, CNRS–UMR 5182, Lyon, France

^cCNRS, INSA Lyon, LaMCoS, UMR5259, 69621 Villeurbanne, France

* Corresponding author: email address: andre.schroder@insa-lyon.fr

Abstract

As the primary products of lipid oxidation, lipid hydroperoxides constitute an important class of lipids generated by aerobic metabolism. However, despite several years of effort, the structure of the hydroperoxidized bilayer has not yet been observed under electron microscopy. Here we use a 200 kV Cryo-TEM to image small unilamellar vesicles (SUVs) made i) of pure POPC or SOPC, ii) of their pure hydroperoxidized form, and iii) of their equimolar mixtures. We show that the challenges posed by the determination of the thickness of the hydroperoxidized bilayers under these observation conditions can be addressed by an image analysis method that we developed and describe here.

keywords: lipid bilayers, hydroperoxidation, small unilamellar vesicles, cryo-TEM.

ARENA

Hydroperoxidation of an unsaturated lipid chain results in the chemical grafting of an organic hydroperoxide (-OOH) at the immediate vicinity of one unsaturation. This induces strong changes in the structure and properties of the bilayer, as we and others have shown (Wong et al., 2007; Heuvingh, & Bonneau, 2009; Weber et al., 2014; De Rosa, Spinozzi, & Itri, 2018; Junqueira et al., 2021; Paez-Perez et al., 2023). But the hydroperoxidized lipid bilayers have never been imaged at the molecular level. Here we present results from the observation by electron microscopy of POPC and SOPC bilayers with different hydroperoxidation degrees.

High resolution electron microscopy images of phospholipid bilayers suspended in water are ideally obtained from cryo-transmission electron microscopy (Cryo-TEM). Small unilamellar vesicles (SUVs) of 30-100 nm in diameter, that can be assembled from a known composition of phospholipids, are the preferred objects for the observation of bilayers by Cryo-TEM. Phospholipid bilayers display a typical thickness of 3-5 nm, roughly a factor of ten above the best resolution of Cryo-TEM technology, which is below 0.5 nm. The resolution of this electron imaging technique depends mainly on three factors, namely the acceleration voltage of the

electrons or electron potential, the overall lens system, and the CCD detection camera (direct detection versus CMOS detector or ssCCD). Developments of the TEM technology over the last decades have improved in those three aspects. The electron beam potential V that governs the beam wavelength λ , has evolved from less than 100 kV in the sixties to 300 kV nowadays (Chua et al., 2022). Also, both the quality of the objective lens system, crucial since it limits in practice the resolution to ~ 0.1 nm, and the quality of the CCD sensors of the detection cameras, have constantly evolved over the years. Hence, the resolution of most recent Cryo-TEMs is not only high enough to enable measuring the average thickness of a phospholipid bilayer, but it is now possible to identify lipid domains in a multicomponent membrane where phase separation takes place, through the evaluation of the local membrane thickness (Heberle et al., 2020).

Challenges

The evaluation of the local bilayer thickness, which can be comfortably achieved on a 300 kV TEM (Heberle et al., 2020), poses a fundamental challenge for medium to low resolution instruments, of 200 kV and less. But the last generation of Cryo-TEM instruments does not make up the majority of the fleet in use in laboratories, 100 kV and 200 kV Cryo-TEMs being still mostly in use. It is also expected that only a small fraction of groups will benefit from the latest developments in this technology over the next few years, since the lifetime of a Cryo-TEM exceeds 20 years, and the last generation of 300 kV machines are relatively costly. Altogether, those factors will naturally limit the turnover of the instruments. It is thus important to develop methods that allow to explore the limits of the information contained in bilayer images from medium resolution Cryo-TEMs.

Typical Solutions

Image analysis methods are typically based on image filtering that decreases the intrinsic noise of an EM image, the result being thus closer to the characteristics of the bilayer. Image filtering can be isotropic, as obtained from regular FFT or Gaussian filtering, or can be based on local oriented filtering that exploits the membrane geometry as a strongly anisotropic medium with different in-plane and normal-to-the-plane organization. In the present case, we focus on the development of an image analysis of the latter type.

MEMBRANE PROFILE IMPROVEMENT BY SELECTIVE RADIAL ALIGNMENT

Main idea

The present work aims at delivering a reliable method for measuring the bilayer thickness of SUVs imaged with a medium to low resolution Cryo-TEM. The general idea is that of an algorithm that performs oriented averaging of the image along the membrane SUV contour, with **i)** a selectivity criterium based on the local, pixel range noise in the image, so that regions of the contour that do not contain sufficient information about the bilayer profile are removed, together with **ii)** a recursive process improving the measure with a convergence routine. Note that averaging methods exist for perfectly round-shaped objects, as for example the one available as a plugin in the Image J software (<http://questpharma.u-strasbg.fr/html/radial-profile-ext.html>). Here, the proposed method not only accounts for SUVs not being perfectly round shaped, but it also rejects noisy regions that tend to blur or smooth the gray level average profile of the bilayer, on which is based the thickness evaluation.

BEFORE YOU BEGIN

In this section, we describe the different steps leading to the Cryo-TEM images required to determine lipid bilayer thickness. Briefly, hydroperoxidized forms of the desired lipids (POPC and SOPC) are first prepared (Lafarge et al., 2023), followed by the formation of SUVs of the desired composition. Suspensions of SUVs are then frozen and observed under a 200 kV TEM microscope. As a result, we collect digital images from the liposomes that are then analyzed by our method.

KEY RESOURCES TABLE

REAGENT or RESOURCE	SOURCE	IDENTIFIER
Chemicals, Peptides, and Recombinant Proteins		
Methylene Blue	MERK	PHR3838-1G
Phospholipids POPC and SOPC	MERK	850457P-25MG, 850467P-25MG
CD ₃ OD (deuterated methanol)	MERK	422878-10ML
Software and Algorithms		
Python software	https://www.anaconda.com/download	
ImageJ software	https://imagej.net/downloads	
Other		
Irradiation Lamp 656 nm	Intelligent LED Solutions, UK	ILR-ON12-RED1-SC211-WIR200
Cellulose membrane dialysis tubings, 0.5 cm diameter, molecular cut-off 14000 Dalton	Sigma Aldrich	D2272-5ft

Table 1 Key resources for implementing the method in this paper.

MATERIALS AND EQUIPMENT

The section details the materials requested for lipid hydroperoxidation (see also Table 1) and for liposome fabrication. It also describes how liposomes are cryogenized, and observed under our 200 kV Cryo-TEM microscope.

Materials

1-palmitoyl-2-oleoyl-glycero-3-phosphocholine (POPC, 16:0-18:1) and 1-stearoyl-2-oleoyl-glycero-3-phosphocholine (SOPC, 18:0-18:1) were purchased in chloroform (25 mg/mL) from Avanti Polar Lipids. Lipids were stored at -20°C and used without further purification. Methanol-D₄ (CD₃OD) with 99.8 % D, was purchased from Acros Organics, and 1,9-dimethyl-methylene blue (MB) was provided as powder from Sigma Aldrich. A 6 mM stock solution of MB in CD₃OD was prepared. Hydroperoxidation was performed in a homemade box chamber equipped with 48 red LEDs ($\lambda=656$ nm, delivering 9 Watts each), corresponding to a light power density of 600 W.m⁻², provided by ILS (Intelligent LED Solutions). During illumination, the chamber was kept under constant ventilation to remove heat excess. Cellulose membrane dialysis tubings (diameter=0.5 cm) with a molecular cut-off of 14000 Da were purchased from Sigma Aldrich. All nuclear magnetic resonance (NMR) spectra were recorded on an Avance 400 spectrometer (Bruker, Germany) at 298 K. Chemical shifts (δ) were referenced from residual methanol (3.31 ppm in ¹H NMR).

Lipid hydroperoxidation

The two hydroperoxidized isomers of POPC and SOPC, named POPC-OOH and SOPC-OOH respectively, shown in Fig.1, were synthesized according to a photochemical reaction, using MB as a photosensitizer. In a test tube, 6 mL of a [10 mM phospholipid + 50 μ M MB solution in CD₃OD] was prepared using the previously dried phospholipids and the MB stock solution. Before illumination, quick control of the lipid quality was made by NMR, by comparing to standard published spectra (Gardner & Weisleder, 1972). The solution was then exposed to red light illumination (LED, see Table 1) under constant oxygen flow provided by a bubbling needle and magnetic stirring to reach the full conversion in less than 10 min. The conversion rate was followed by NMR.

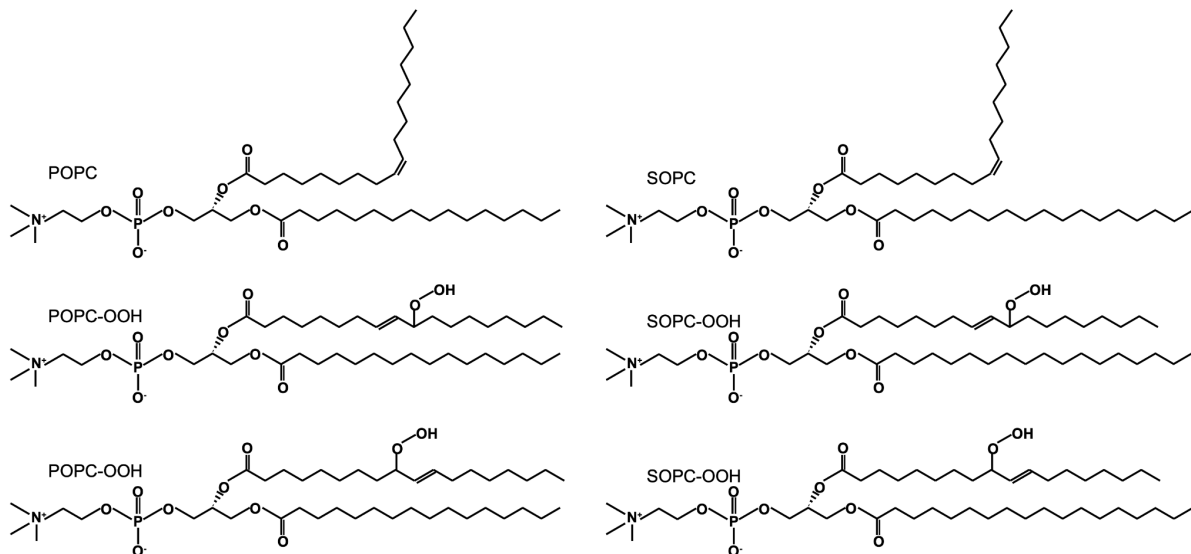


Fig. 1 Chemical formula of POPC and SOPC with their two respective hydroperoxidized isomers.

Once full hydroperoxidation was reached, MB was removed by dialysis. For that, 1 mL of the hydroperoxidized lipid-in-MB solution was evaporated and then redispersed in 2 mL of Milli-Q water, to reach a concentration of \approx 2.5 mg/mL, forming a LUV dispersion, that was placed inside a washed dialysis tubing of 15 cm length (see Table 1). The dialysis was performed against 800 mL of Milli-Q water, under constant stirring at ambient temperature, for 3 h. The free of MB LUV dispersion was then dried using a rotary evaporator, and lipids were then redispersed in CD₃OD, and controlled by NMR. Hydroperoxidized lipids in CD₃OD were kept at -20°C for further use. Initially encapsulated MB in the SUVs certainly remains, at least partly encapsulated after that dialysis step; we argue that this does not influence further measurements.

Liposome preparation

Six types of liposome dispersions were studied, corresponding, for each of the lipids POPC and SOPC, to 0 mol%, 50 mol% and 100 mol% of hydroperoxidized lipids. For the 50% case, POPC/POPC-OOH (resp. SOPC/SOPC-OOH) in CD₃OD mixtures were first prepared by mixing appropriate volumes of the corresponding lipid-in-CD₃OD mother solutions. For each 50/50 (target) mixture, the exact fraction of hydroperoxidized lipid was checked by ¹H NMR. Starting from the lipid-in-CD₃OD solutions, liposomes were prepared as follows: 5 mg of lipids corresponding typically to 500 μ L of the 10 mg/mL in CD₃OD solution, were placed in a 5 mL round bottom flask and dried by rotary evaporation under reduced pressure. The resulting dry film was hydrated with 1 mL of milli-Q water and stored at 6°C for 48 h. The sample was then sonicated a first time with a micro-tip (Fisherbrand) (with a signal amplitude corresponding to 1% of the maximal amplitude, the tip emitting at its resonance frequency) for 2 to 8 min depending on the lipid (see Table 2) to form Small Unilamellar Vesicles (SUVs). The sample

was afterward extruded through a polycarbonate filter (Whatman Nuclepore) of 0.8 µm pore size, using a mini extruder (Avanti Polar Lipids) to break vesicle aggregates. The solution traveled 21 times through the polycarbonate filter. Finally, depending on the lipid composition, some samples were sonicated, to obtain a satisfactory fraction of ≈100 nm SUVs, as further checked by Cryo-TEM observation. All the SUV solutions were stored at 6°C before being analyzed by Cryo-TEM.

Lipid	1^{rst} sonication time (min)	2^{nd} sonication time (min)
POPC	2	2
POPC-OOH/POPC (50/50)	2	2
POPC-OOH	3	-
SOPC	8	6
SOPC-OOH/SOPC (50/50)	3	-
SOPC-OOH	2	-

Table 2 Indicative sonication time to prepare SUVs of each different lipid composition for Cryo-TEM analysis. The first sonication is performed before extrusion and the second sonication (when required) is always performed after extrusion.

Cryo-Transmission Electron Microscopy

Cryo-TEM image acquisition was performed as follows. A 5 µL drop of the previously prepared SUV sample was deposited on a lacey carbon film covered 300 mesh Cu grid (Ted Pella) previously rendered hydrophilic using an ELMO glow discharge unit (Cordouan technologies). The sample was placed inside a homemade chamber held at 22°C and 80 % RH (relative humidity). The excess sample was removed using a filter paper to obtain a film thinner than 500 nm. The sample was then rapidly immersed into liquid ethane (held at -190°C using liquid nitrogen, resulting in a fast cooling rate ≈10000 K/s) to obtain a frozen sample preserving the native structure of the vesicles and avoiding the formation of ice crystals. The grid was mounted onto a cryo-holder (Gatan 626) and observed under low dose conditions ($10 e^- / \text{Å}^2$) in a Tecnai G2 microscope (FEI) at 200 kV. The sample inside the microscope was left at least 20 min at -170°C before image acquisition. Images were acquired using an Eagle slow scan CCD camera (FEI). Under these conditions, images with a pixel size of 0.439 nm were obtained, and those containing at least one SUV were kept for analysis. Those images are named original images in the following.

Choice and preparation of Cryo-TEM images

Fig. 2 shows a typical Cryo-TEM image, here of POPC SUVs. From such images, spherical unilamellar SUVs are selected for analysis. In ImageJ, the circle tool is first used by hand to choose the contour of a selected SUV, with radius R and center C_0 . Then a square is cropped with size $L = 2R + 80$ pixels, centered on C_0 . Error on both R and C_0 is typically below 3 pixels,

mainly due to lack of perfect circularity of the SUV. The figure shows also a typical SUV selected for image cropping using this procedure.

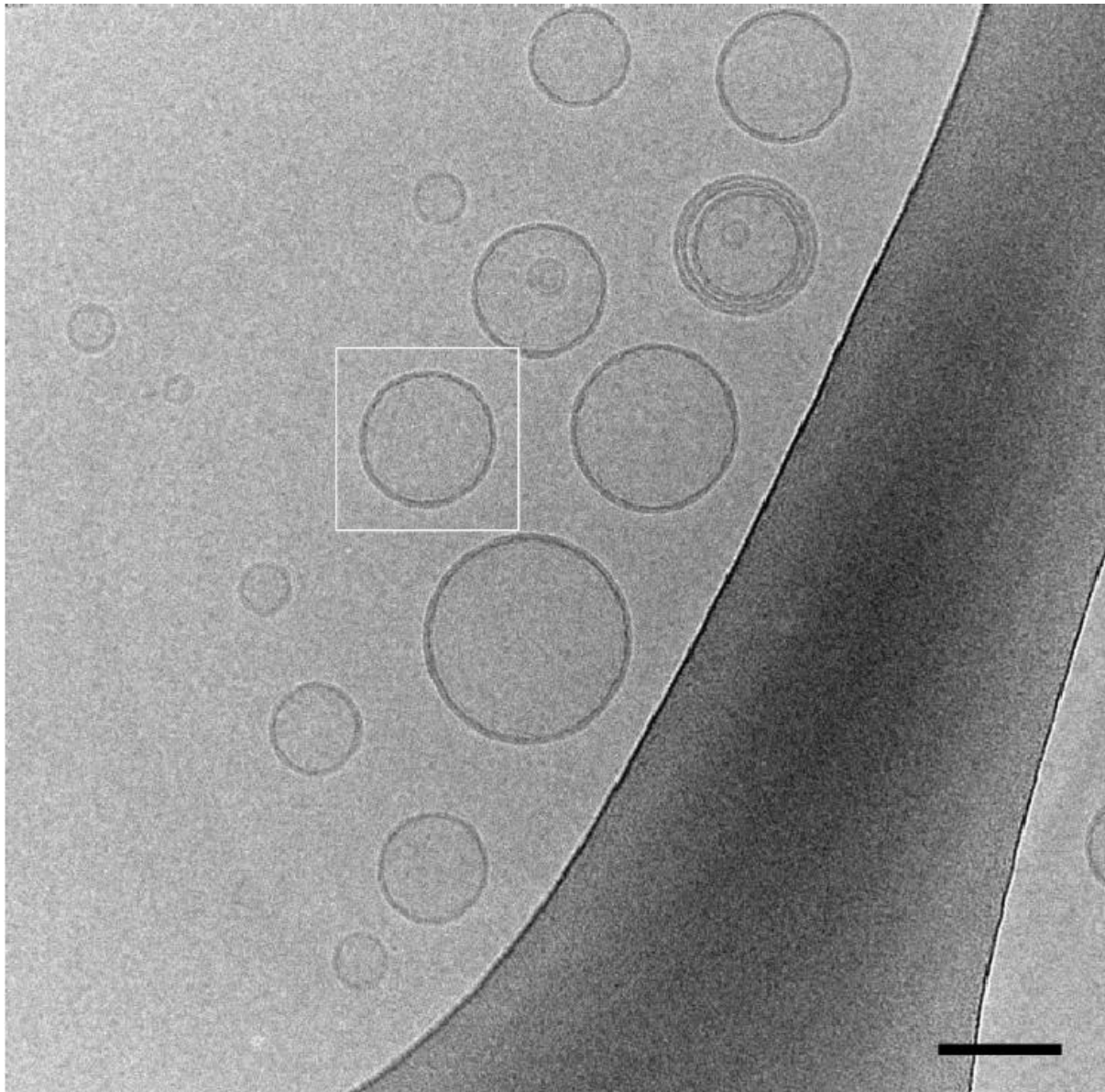


Fig. 2 Original Cryo-TEM image showing several SUVs of POPC. The white square is centered on a selected circular SUV of radius R and center C_0 as determined using the circle tool in ImageJ. From that square, of size $L = 2R + 80$ pixels, a new image is saved for analysis by the method described in this paper. Scale bar is 100 nm.

STEP-BY-STEP METHOD DETAILS

Here we describe a script, coded in Python, that measures the average bilayer thickness of an SUV imaged with a medium resolution Cryo-TEM. The goal of the script is to deliver the best possible gray level average profile in the direction normal to the bilayer, from which the bilayer thickness is directly evaluated (Heberle et al., 2020).

Step 1: image acquisition

SUVs are treated one by one. As explained above, an original image typically containing several SUVs (see Fig. 2 for an example) is opened in ImageJ, from which one or more isolated SUVs will be selected and cropped. Preferred SUVs are the ones isolated from neighboring SUVs and the carbon grid, enabling bilayer profile analysis over 2π radians of the contour. Analysis of a bilayer profile over a restricted angular domain is also possible, although not presented here. Each square sub-image (see Fig. 3A) containing one SUV of interest is treated individually by the Python script. Gray levels $I_{x,y}$ (integer numbers, 14 bits) are stored in a (L,L) matrix, with X (resp. Y) = $0..L-1$ corresponding to the integer coordinates of the image pixels.

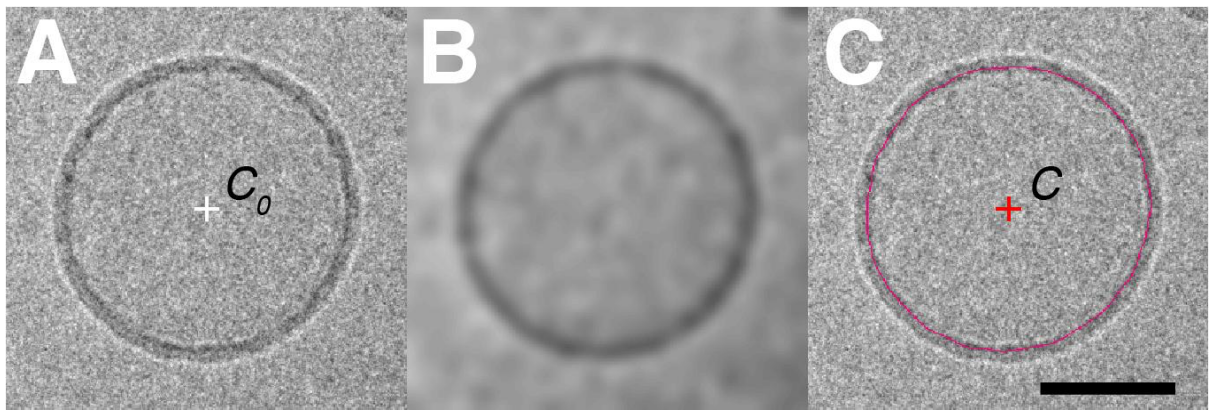


Fig. 3 Determining the contour of SUVs in cryo-TEM images. **A** Isolated SUV, as extracted by cropping an original Cryo-TEM image, as depicted in Fig. 2. The cross indicates the image center C_0 . Image size in pixels is $L \times L$, with $L = 2R + 80$, with R the radius of the vesicle in pixels as determined by the circle tool in ImageJ. **B** A Gaussian blur of the original SUV. **C** Zero order contour on the original image, with the associated center of mass C . Scale bar is 50 nm.

Step 2: computing gray level profiles by oversampling

Since the gray level values of the image contain the relevant physical information about the atomic distribution defining the liposome, one needs to obtain accurate representations of the image pixels, despite noise and other perturbation factors. Here we choose to oversample the gray level values along a given radial direction. We will work with straight segments \mathbf{s} , with a length of 60 pixels, centered at the membrane contour. Along \mathbf{s} , we compute the coordinates (x_p, y_p) of six hundred points \mathbf{P}_p , equally distributed along the segment, corresponding to an oversampling of a factor ten of the image resolution. The distance between two neighboring points \mathbf{P}_p and \mathbf{P}_{p+1} is thus 0.1 pixel, see Fig. 4A. We then associate to each oversampling position \mathbf{P}_p a pseudo-pixel of size 1 pixel (Fig. 4B) and intensity I_p given by a simple interpolation:

$$I_p = I_{x,y} a^- + I_{x+1,y} a^{+-} + I_{x,y+1} a^+ + I_{x+1,y+1} a^{++} \quad (1)$$

where X and Y are the integer parts of the real coordinates x_p and y_p of \mathbf{P}_p respectively. The four values a^- , a^{+-} , a^+ and a^{++} in Eq. (1) correspond to the respective area fractions occupied by \mathbf{P}_p on the four original pixels of coordinates (X, Y) , $(X+1, Y)$, $(X, Y+1)$, and $(X+1, Y+1)$ that \mathbf{P}_p covers, as shown in Fig. 4C. For building up intuition a few radial profiles, determined by oversampling at the level of the SUV membrane shown in Fig. 3A, are displayed in Fig. 5.

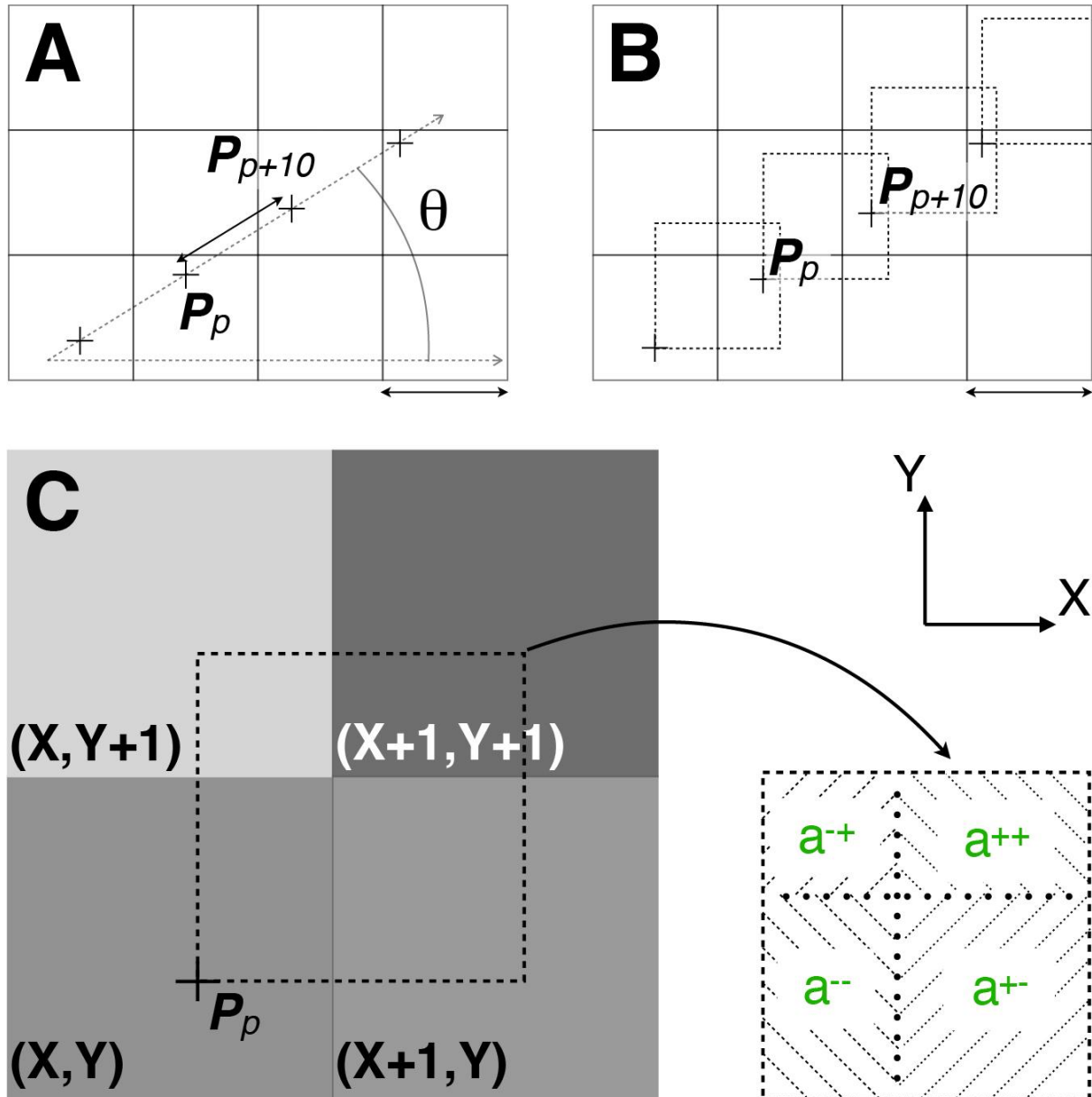


Fig. 4 Oversampling of a gray level profile. **A** A region of the original (L, L) matrix that contains the image. The direction of a \mathbf{s} segment, oriented at the angle θ with the x-axis is shown in dots. Crosses (+) represent some of the points \mathbf{P}_p along \mathbf{s} . Here we show as an example \mathbf{P}_p and \mathbf{P}_{p+10} that are spaced by a distance of 1 pixel size. **B** Same region, with the pseudo-pixels associated with the few points \mathbf{P}_p shown by crosses in A. **C** One particular pseudo-pixel (dotted square) and the four original pixels in which it is embedded, with the corresponding area fractions occupied by the pseudo-pixel. Arrows in A and B show 1 pixel length.

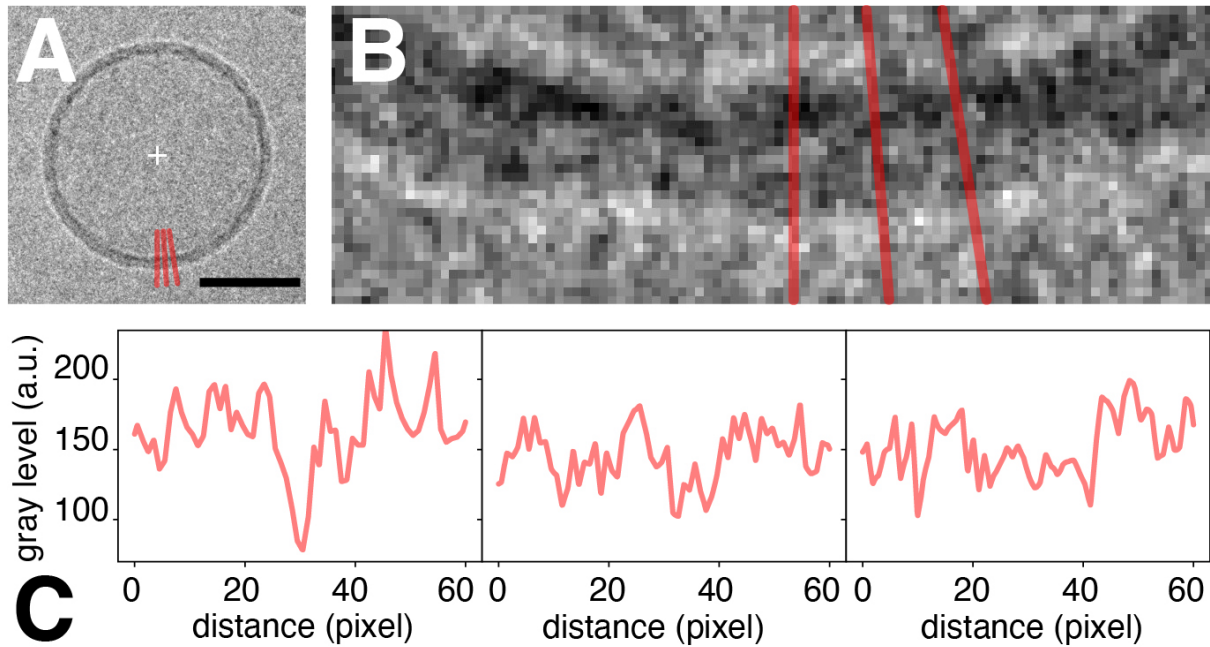


Fig. 5 Profiles of gray levels across the SUV membrane. **A** The position of three segments \mathbf{s} drawn radially across the membrane of Fig. 3A. Scale bar is 50 nm. **B** Zoom around the three segments, showing clearly each pixel. **C** The corresponding gray level intensity profiles I_p as calculated from Eq. (1).

Step 3: determining the SUV contour

In order to detect the membrane contour, a Gaussian filter (blur) is first applied to the image, generating a darker region along the perimeter, roughly at the level of the phosphate heads of the inner bilayer leaflet, see Fig. 3B. The oversampled intensity I_{ip}^{blur} is then computed according to Eq. (1) along a set of n radial segments \mathbf{s}_i ($i=0..n-1$) of the blurred image with center at C_0 and orientation θ_i – see Fig. 4A. n is the integer number of pixels in the initial perimeter of the circle determined in ImageJ, about 800 for the present image, and typically in the range 600 - 1500 for the SUVs that we measured in this paper. The azimuthal orientation of each radial segment differs thus by an angle $\delta\theta=2\pi/n$. All radial gray level profiles extracted along the n \mathbf{s}_i segments display a minimum at the membrane level. We choose the n values of such minima as the position of the SUV contour. Fig. 3C shows the contour determined by this method superimposed to the original SUV image.

Step 4: determining radial profiles.

In this step all radial profiles I_{ip} are computed along n segments \mathbf{s}_i centered at C , from the original (non blurred) SUV image, see Fig. 6 that displays also the average $\bar{I}_p = \langle I_{ip} \rangle$. \bar{I}_p is expected to exhibit two minima in the case of a perfectly circular SUV imaged with a high enough resolution for the two phosphorus layers to be visible. Often, this can be easily observed from images acquired with a 300 kV EM (Heberle et al., 2020). However, due to both

the lack of perfect contour determination and noise, the profile is smoothed out by the averaging procedure, making the second minimum less detectable in \bar{I}_p (Fig. 6). In order to better detect the second minimum we introduce an optimization scheme described in the next sections.

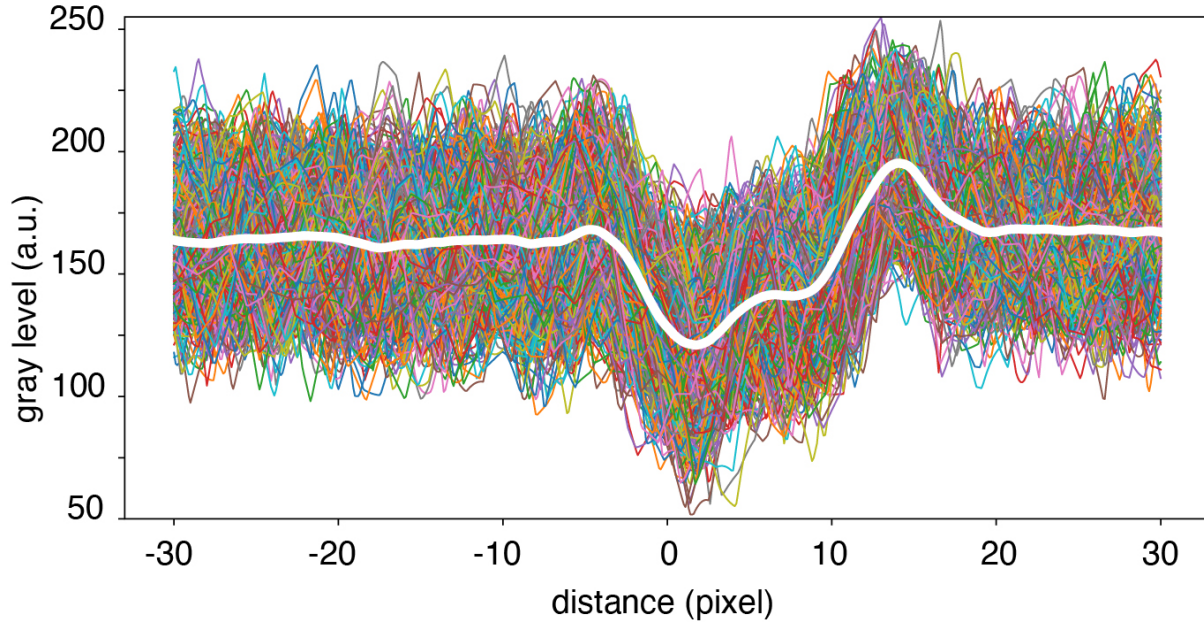


Fig. 6 The set of intensity profiles I_{ip} calculated directly from the acquired image (colored lines), and their average profile \bar{I}_p^0 (white circles).

Step 5: determining bilayer thickness

The average of the gray level profiles - see Fig. 6 - displays in general two minima as other profiles from typical TEM images of SUVs (Heberle et al., 2020). The average profile is fitted in the region of each of the two minima with a polynomial of degree 2, providing the two minima positions r_1 and r_2 . The distance r_2-r_1 , often named D_{TT} for the trough-to-trough distance, has been shown to be simply related to D_{HH} , the headgroup-headgroup distance, for a number of common lipids with various hydrocarbon chain lengths (Heberle et al., 2020). Typically, one finds $D_{HH} = D_{TT} + 0.6$ nm. We will now adopt the quantity D_{HH} as a measure of the membrane thickness h .

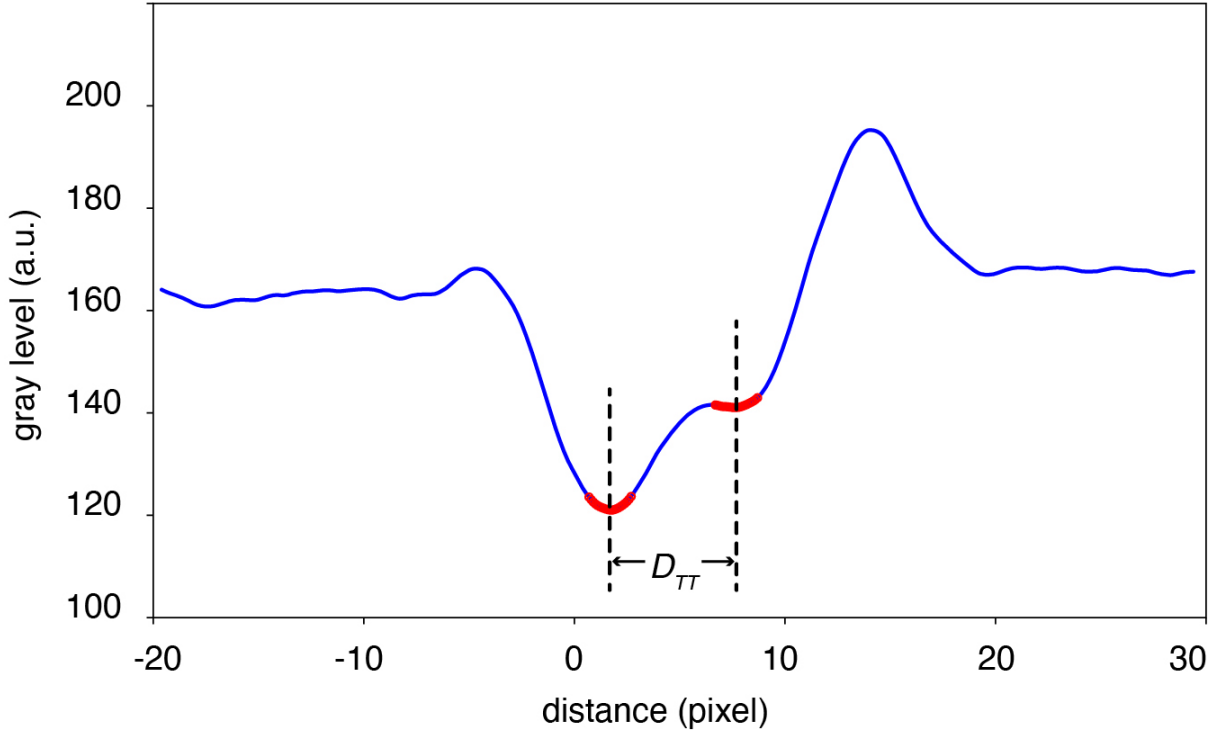


Fig. 7 The trough-to-trough distance D_{TT} is measured from the two minima in the average profile, here $D_{TT} = 5.75$ pixels from \bar{I}_p^0 of Fig. 6. Better determination of the minima can be achieved by improving the average profiles as explained in this paper (see Step 6.)

Step 6: improving average profile determination

Several reasons can lead to an average profile with less marked minima. The most important one is the lack of perfect determination of the SUV contour, which would smooth out even noiseless profiles due to a wrong (displaced) relation between radius and z position along the membrane normal. Here, in step 5 we introduce an optimization loop to improve the average profile. We achieve this by “sliding” each profile along the radial direction in order to find its optimal position. Optimization is achieved by maximizing at iteration k a measure of the correlation between a given profile and the average computed at iteration $k-1$. The correlation between any I_{ip} at iteration k and $\bar{I}_p^{[k-1]}$ for any k is obtained through a radial sliding procedure of each I_{ip} . More precisely, each I_{ip} is slid back and forth along the θ_i direction, in the limit range of ± 4 pixels, with a one tenth of pixel step, and the correlation c_{im} is calculated for each sliding position m as:

$$c_{im} = \frac{1}{(j_f - j_0)} \sum_{j=j_0}^{j=j_f} \bar{I}_j^{[k-1]} I_{i(j+m)} w_m \quad (2)$$

with k the iteration number, m the sliding index ranging from -40 to +40, $j_0 = \max(0, m)$, $j_f = \min(600, 600+m)$ and w_m a gaussian weighting function that centers the correlation over the width of the dark groove. Division by $j_f - j_0$ normalizes the correlation over the length of the correlation window. For each θ_i one determines the best m_i value as the one leading to the largest c_{im} . At the end of each run k , one thus obtains for each profile i a pair of values (m, c_{im}) .

To initiate the iteration we correlate all profiles I_{ip} with \bar{I}_p^0 . The result of this alignment procedure is shown in Fig. 8 for a typical SUV at step $k=1$. The sliding values m are distributed around 0, which corresponds to the original contour. The correlation factors c_{im} are also distributed around some average value. Improvement of the profile under our approach is obtained by restricting the profiles used for computing the new average \bar{I}_p^k at step k to those within some subspace of (m, c_{im}) . Although more sophisticated approaches can be taken implying restriction regions of different shapes along both the c_{im} and m axis, we found empirically that the restriction $-1 < m < 1$, i.e. choosing as relevant for the average all profiles which are within one pixel of an optimal alignment with the reference profile, leads to a fast convergence.

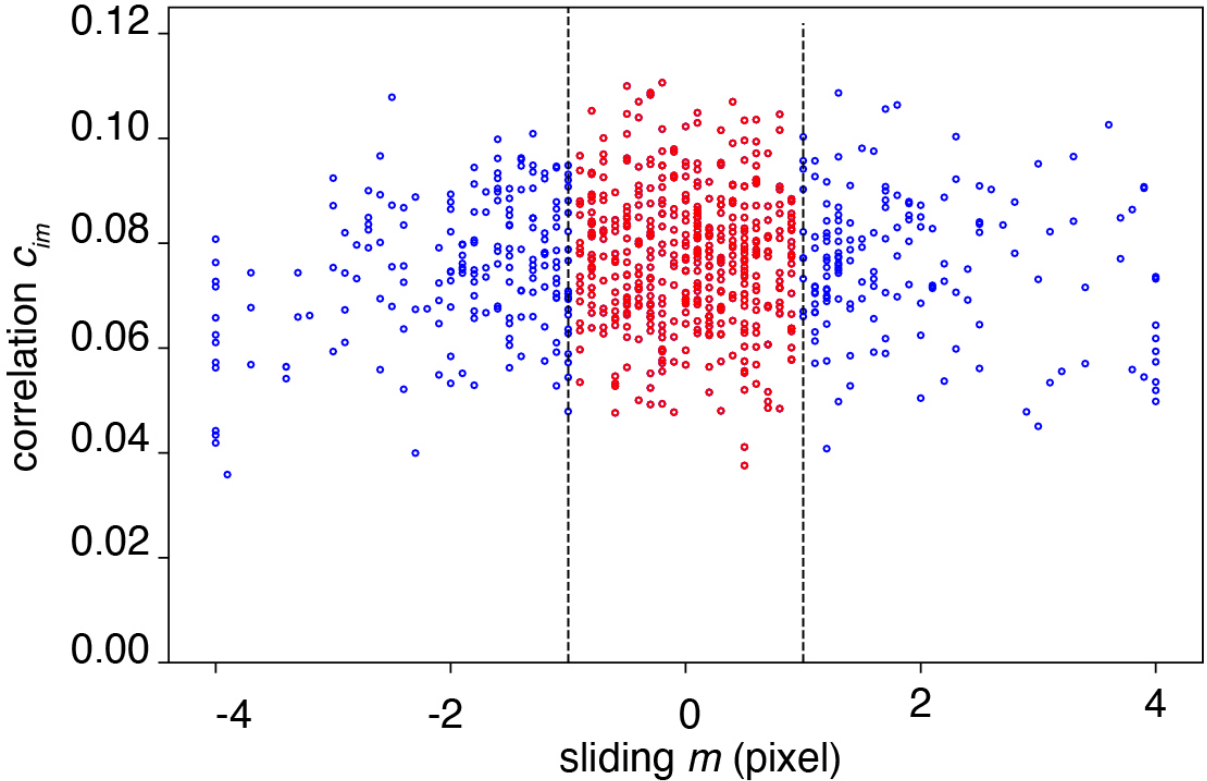


Fig. 8 The phase space (m, c_{im}) of the alignment procedure at iteration k (here at $k=1$, for the SUV of Fig. 3). The average profile at iteration $k+1$ is computed from the restriction $-1 < m < 1$.

The iteration proceeds by correlating at step $k+1$ all profiles I_{ip} with the average $\bar{I}_p^{[k]}$, applying the same restriction to the (m, c_{im}) space. The iteration is carried on until one reaches the desired accuracy for the relevant quantity being measured. In our case we determine the bilayer thickness h as discussed in Step 5 above. At each step k of the iteration, one determines thus a value h_k and the iteration procedure is stopped when h_k converges to some limit value. In practice we stop here the iteration when $-0.01 < 1-h_k/h_{k-1} < 0.01$, see Fig 9.

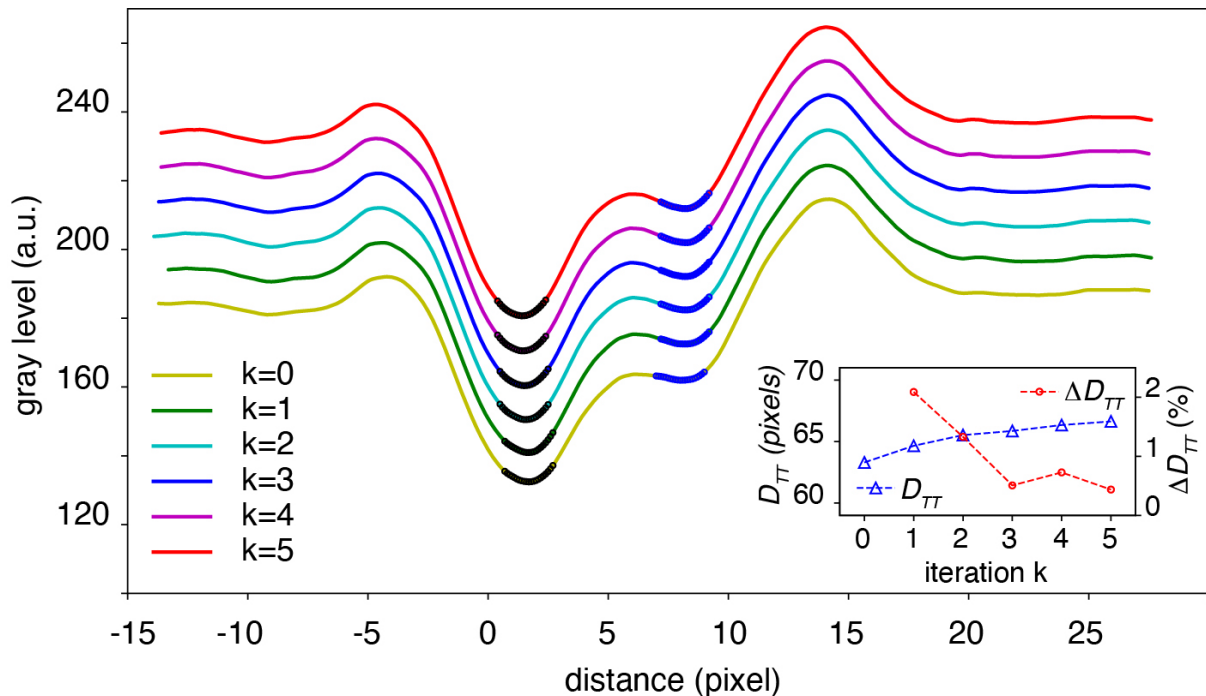


Fig. 9 Gray level profiles from the procedure discussed in this paper, from the reference profile ($k=0$) to iteration $k=5$. Profiles were displaced vertically by an arbitrary amount for clarity. **Inset.** Evolution of the trough-to-trough distance $D_{TT}^{[k]}$ and of its relative increments $\Delta D_{TT}^{[k]} = (D_{TT}^{[k]} - D_{TT}^{[k-1]}) / D_{TT}^{[k-1]}$. The iteration is stopped when $\Delta D_{TT}^{[k]} < 0.01$.

EXPECTED OUTCOMES

Measurement of the lipid bilayer thickness

We selected more than fifty high resolution TEM images with size $0.9 \times 0.9 \mu\text{m}^2$ for each of the six phospholipid compositions that we name P₁₀₀, PO₅₀, PO₁₀₀, S₁₀₀, SO₅₀, and SO₁₀₀: P₁₀₀ for pure POPC, PO₁₀₀ for pure hydroperoxidized POPC, PO₅₀ for a 50-50 mixture of the two, while samples named with S refer identically to SOPC and its hydroperoxidized forms. This corresponded to hundreds of individual SUVs, with various shapes, sizes, and lamellarities. Based on a naked-eye assessment, only a fraction of those SUVs were selected for numerical treatment with our Python script, corresponding to SUVs with sufficient contrast and sharpness, so that the two phosphorus leaflets appeared visible along a significant portion of their perimeter. Fig. 10 shows typical analyzed EM images. We selected between 17 and 41 SUVs for each lipid composition, except for P₁₀₀, for which only 8 vesicles were retained, due to a systematic lower contrast in the images, *i.e.* with the two leaflets often not detectable.

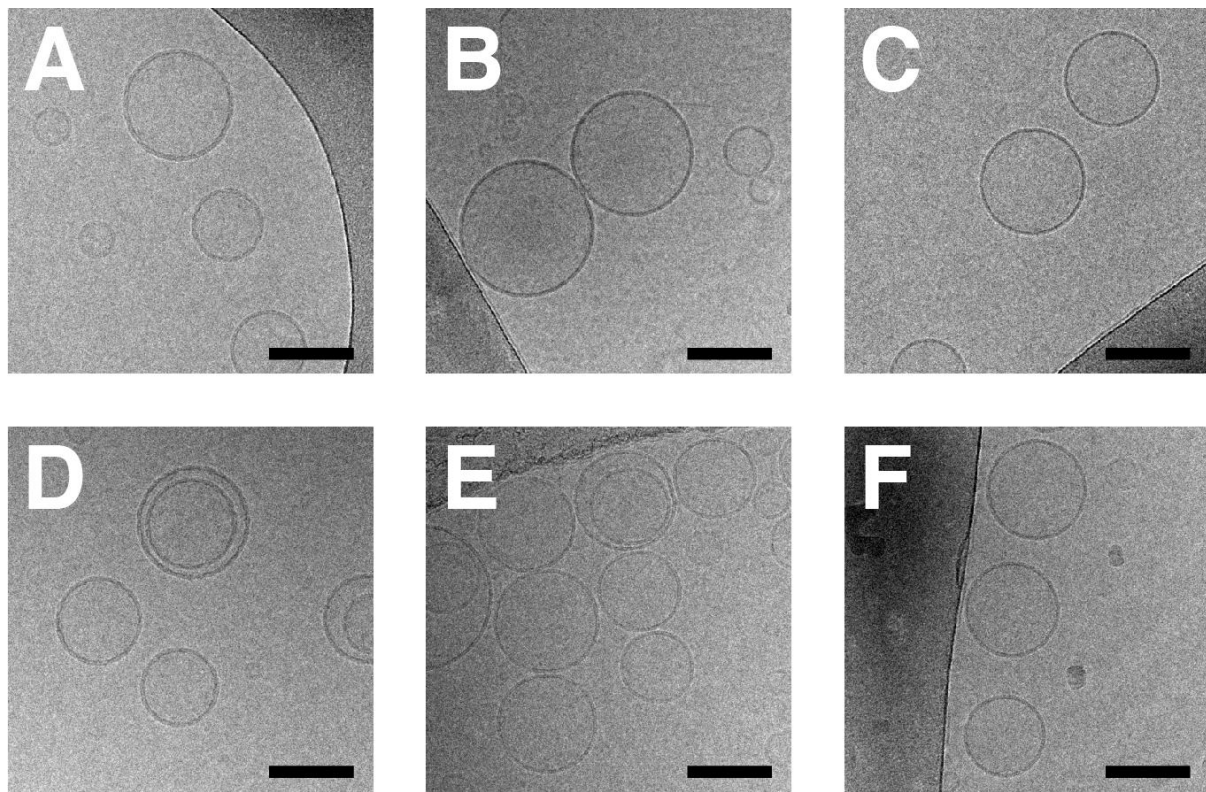


Fig. 10 Examples of images from each sample studied by Cryo-TEM. **A** P₁₀₀. **B** PO₅₀. **C** PO₁₀₀. **D** S₁₀₀. **E** SO₅₀. **F** SO₁₀₀. Scale bar is 100 nm.

Selected SUVs were analyzed as described above. Membrane thicknesses h are presented in Fig. 11 as violin plots, revealing their statistical distribution. The values for POPC and SOPC compare well to published values, as shown in Table 3.

lipid	h (nm) from literature	h (nm) this paper	Δh (%) from literature	Δh (%) this paper
POPC	3.70 nm (Kucerka et al., 2005)	3.69 ± 0.06	- 20 (De Rosa et al., 2018)	- 22
SOPC	3.90 nm (Greenwood et al., 2008)	3.98 ± 0.07	-	- 26

Table 3 h values for POPC and SOPC, as found in literature and as calculated here, and relative decrease Δh (full hydroperoxidation) of the bilayer thickness.

For membranes assembled from the hydroperoxidized forms of POPC and SOPC, we found that h decreases linearly with the fraction of hydroperoxidized lipids in the bilayer. Fully hydroperoxidized bilayers display a thickness reduction Δh of the order of 20-30%, see also

Table 3. For POPC this compares well to the 20% decrease measured by *De Rosa et al.* using X-ray scattering (De Rosa, Spinozzi, & Itri, 2018). For SOPC the thickness of hydroperoxidized SOPC bilayers has not been measured before.

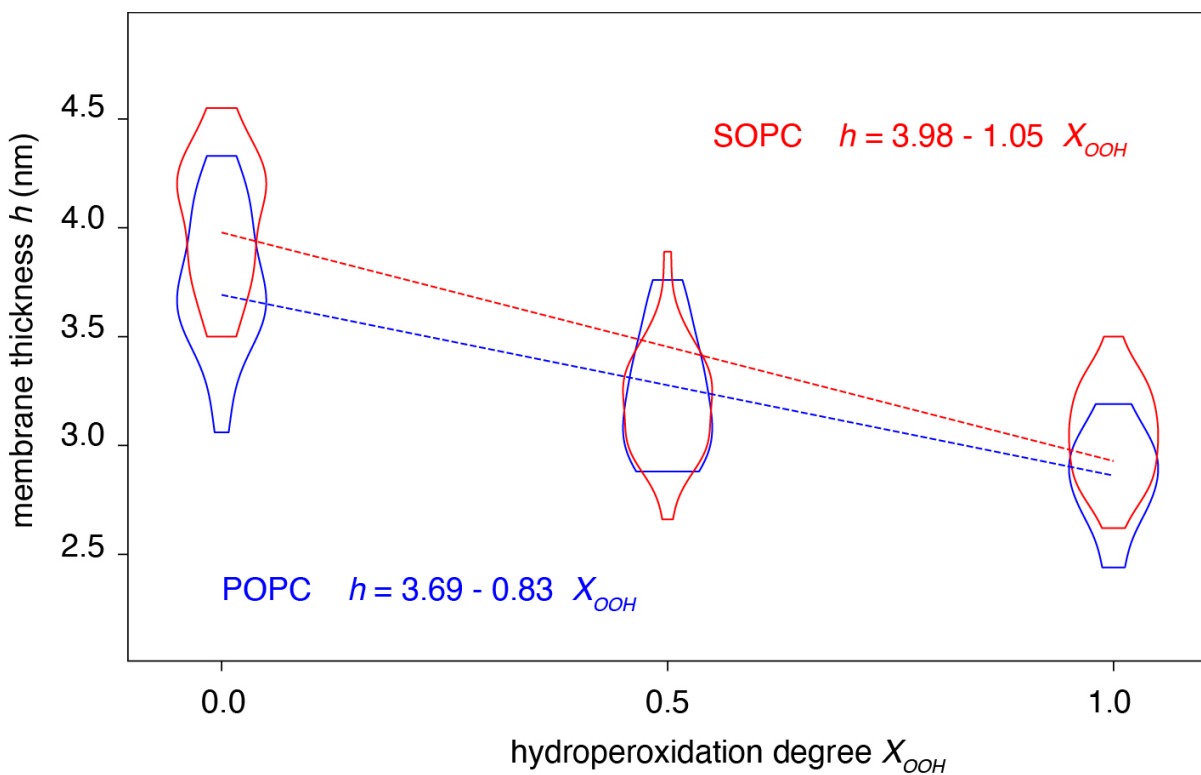


Fig. 11 Average bilayer thickness h measured from cryo-TEM images of SUVs of POPC and SOPC, as a function of X_{OOH} , the fraction of hydroperoxidized lipids in the bilayer. The best linear trend of the variation of h average values with X_{OOH} is also given for the two lipids.

CONCLUSIONS AND CONNECTIONS

We provided here not only the first cryo-TEM images of hydroperoxidized lipid bilayers, but also the first image-based measurements of their thickness. The physical principles of image formation under transmission electron microscopy have been known for a long time (Tahara, & Fujiyoshi, 1994), but only recently have they been operationally applied to the determination of lipid bilayer thickness from SUVs (Wang, Bose, & Sigworth, 2006). We now discuss our method and findings in the context of other measurements of lipid bilayer thickness, by cryo-TEM or by X-ray and neutrons scattering, which are also discussed in chapters “Phase separation in model lipid membranes investigated with cryogenic electron microscopy” and “Structure of symmetric and asymmetric lipid membranes from joint SAXS/SANS” of this MIE volume.

In simple terms, the image captured by a cryo-TEM measurement derives from the convolution of the instrument function (an oscillatory function named the contrast transfer function CTF)

with the 2D plane projection of the 3D electron phase shift function γ . The phase shift function expresses the ability of the sample to phase-shift the wavefunction of the electron beam. It is related to the sample atomic distribution (different atoms lead to different electron phase shifts) and to the electrostatic field in the sample. Due to symmetry and isotropy of the atomic distribution in the SUV bilayer, the relevant component of γ is its variation across the membrane thickness: it has a maximum at the level of the phosphate heads of each leaflet and a minimum in the middle of the membrane. The gray-level profiles extracted from the images, are thus the result of a projection and a convolution of γ . Despite the linear nature of these mathematical transformations, they involve two kernels that select which features of γ would eventually show up in the profile even in an ideal case of high resolution and absence of intrinsic noise. For conventional lipids it has been shown that for high-resolution EM the features in γ translate well to the distance between dark grooves in the SUV images, allowing in that case to “read” the membrane thickness directly from the images.

In this work we showed how to extend this process to medium-resolution (200 kV) EM, where the membrane dark grooves in the SUV images are less marked and noisier. For POPC we found that our image treatment, carefully optimizing the radial position of the gray-level profiles, leads to values comparable to those extracted from high-resolution measurements. For SOPC we provide the first membrane thickness determination from cryo-TEM images, and its value compares well with values from other techniques.

Hydroperoxidized lipids have quite distinct molecular chain conformations with, in particular, a high number of snorkeling loops that re-arrange the carbon and hydrogen atoms in the vertical direction (Paez-Perez et al., 2023). Our images show nevertheless that γ keeps, under hydroperoxidation, enough contrast between its two maxima and its central minimum to allow for a clear identification of two leaflets. And if one accepts that the distance between the two minima in the gray level profiles are still a measure of the bilayer thickness, we find that its values compare well with published X-ray scattering determinations. Whether or not the simple rule connecting D_{TT} and h still apply for hydroperoxidized bilayers could in principle be investigated by methods discussed in chapter “Phase separation in model lipid membranes investigated with cryogenic electron microscopy” of this volume.

REFERENCES

Chua, E.Y.D., Mendez, J.H., Rapp, M., Ilca, S.L., Tan, Y.Z., Maruthi, K., Kuang, H., Zimanyi, C.M., Cheng, A., Eng, E.T., Noble, A.J., Potter, C.S., & Carragher, B. (2022). Better, Faster, Cheaper: Recent Advances in Cryo–Electron Microscopy. *Annual Review of Biochemistry*, 91, 1–32.

De Rosa, R., Spinozzi, F., & Itri, R. (2018). Hydroperoxide and carboxyl groups preferential location in oxidized biomembranes experimentally determined by small angle X-ray scattering: Implications in membrane structure. *Biochimica et Biophysica Acta (BBA)-Biomembranes*, 1860, 2299–2307.

Gardner, H., & Weisleder, D. (1972). Hydroperoxides from oxidation of linoleic and linolenic acids by soybean lipoxygenase: Proof of the trans-11 double bond. *Lipids*, 7(3), 191-193.

Greenwood, A.I., Pan, J., Mills, T.T., Nagle, J.F., Epand, R.M., & Tristram-Nagle, S. (2008). CRAC motif peptide of the HIV-1 gp41 protein thins SOPC membranes and interacts with cholesterol. *Biochimica et Biophysica Acta (BBA)-Biomembranes*, 1778(4), 1120–1130.

Heberle, F.A., Doktorova, M., Scott, H.L., Skinkle, A.D., Waxham, N.M., & Levental, I. (2020). Direct label-free imaging of nanodomains in biomimetic and biological membranes by cryogenic electron microscopy. *Proceedings of the National Academy of Sciences (PNAS)*, 117(33), 19943-19952.

Heuvingh, J., & Bonneau, S. (2009). Asymmetric oxidation of giant vesicles triggers curvature-associated shape transition and permeabilization. *Biophysical journal*, 97, 2904–2912.

Junqueira, H., Schroder, A.P., Thalmann, F., Klymchenko, A., Mély, Y., Baptista, M.S., & Marques, C.M. (2021). Molecular organization in hydroperoxidized POPC bilayers. *Biochimica et Biophysica Acta (BBA) - Biomembranes*, 1863, 183659.

Kucerka, N., Tristram-Nagle, S., & Nagle, J.F. (2005). Structure of Fully Hydrated Fluid Phase Lipid Bilayers with Monounsaturated Chains. *Journal of Membrane Biology*, 208, 193-202.

Lafarge, E.J., Muller, P., Schroder, A.P., Zaitseva, E., Behrends, J.C., & Marques C.M. (2023). Activation energy for pore opening in lipid membranes under an electric field. *Proceedings of the National Academy of Sciences (PNAS)*, 120 (11), e2213112120.

Paez-Perez, M., Vyšniauskas, A., López-Duarte, I., Lafarge, E., Lopez-Rios De Castro, R., Marques, C.M., Schroder, A.P., Muller, P., Lorenz, C.D., Brooks, N.J., & Kuimova, M.K. (2023). Directly imaging emergence of phase separation in peroxidized lipid membranes. *Communications Chemistry*, 6, 15.

Tahara, Y., & Fujiyoshi, Y. (1994). A new method to measure bilayer thickness: cryo-electron microscopy of frozen hydrated liposomes and image simulation. *Micron*, 25(2), 141-149.

Weber, G., Charitat, T., Baptista, M.S., Uchoa, A.F., Pavani, C., Junqueira, H.C., Guo, Y., Baulin, V.A., Itri, R., Marques C.M., & Schroder, A.P. (2014). Lipid oxidation induces structural changes in biomimetic membranes. *Soft Matter*, 10, 4241.

Wang, L., Bose, P.S., & Sigworth, F.J. (2006). Using cryo-EM to measure the dipole potential of a lipid membrane. *Proceedings of the National Academy of Sciences (PNAS)*, 103(49), 18528–18533.

Wong-ekkabut, J., Xu, Z., Triampo, W., Tang, I., Tielemans, D.P., & Monticelli L. (2007). Effect of Lipid Peroxidation on the Properties of Lipid Bilayers: A Molecular Dynamics Study. *Biophysical Journal*, 93, 4225–4236.